CWI Quarterly Volume 11 (4) 1998, pp. 347 – 369

A Multiresolution Morphological Approach to Stochastic Image Modeling [1]

J. Goutsias
Center for Imaging Science and
Department of Electrical and Computer Engineering
Barton 211, The Johns Hopkins University
Baltimore, MD 21218, U. S. A.
e-mail: goutsias@mycenae.ece.jhu.edu

K. Sivakumar
School of EECS
Washington State University
P.O. Box 642752
Pullman, WA 99164-2752
e-mail: siva@eecs.wsu.edu

We are considering the problem of random image modeling, key to stochastic regularization techniques for image recovery. Our approach treats images as realizations of Gibbs random fields whose energy function takes into consideration geometric information by means of multiresolution morphological constraints. First, morphological operators are used to provide a multiresolution image decomposition. This allows efficient image representation by means of detail error signals. By appropriately constraining these signals, a Gibbs energy function is obtained whose ground states satisfy relevant geometric properties. A few examples illustrate the potential of the proposed approach in image modeling and analysis.

1. Introduction

During the last decade, we have been witnessing a dramatic explosion in visual information. Visual data are acquired in many scientific disciplines, like remote

[1] This work was supported by the Office of Naval Research, Mathematical, Computer, and Information Sciences Division, under ONR Grant N00014-90-1345.

sensing, biology, medicine, geology, and mining. To effectively handle image data, it is important to automate their processing, analysis, and interpretation. In an effort to build "intelligent" devices, capable of automatically performing such tasks, it is necessary to develop algorithms for accurate image manipulation and evaluation. This is the main subject of image processing and analysis [10] which typically employs computers (or special purpose hardware) to manipulate visual data in a discrete form. Abundance of inexpensive computing hardware is mainly responsible for rapid advancements in image processing and analysis software and further advancements in image processing and analysis research.

A large class of image processing and analysis problems involves recovering information about a scene or object of interest from partial or imperfect data. The observed image Y is typically the output of an imaging system applied on an unobserved or hidden image X. As such, Y is a "corrupted version" of X. Our task is to design a suitable algorithm which transforms the observed image Y into a desired image $\hat{X}$ that is as "close" as possible to X. Data Y may be partial due to occlusion or limitations in data collection, and imperfect due to the effect of sensor noise and other artifacts in the imaging system. The inverse problem of recovering X from Y is often *ill-posed* [8] and requires proper regularization.

Regularization is usually done by incorporating *a-priori* information about image X into the problem. A popular approach to regularization, known as *stochastic regularization* [14], uses knowledge about X to mathematically represent images by an appropriately designed probability measure. In particular, a parametric random field model is assumed for X. The success of stochastic regularization obviously depends on available a-priori information and on how well the random field model represents this knowledge [4]. In this framework, statistical techniques are employed to recover X from Y. Stochastic regularization frequently leads to robust and highly effective algorithms for image recovery.

A useful random model for images is a *Gibbs random field* [5]. Gibbs random fields have been extensively used in inverse image processing and analysis problems (e.g., image smoothing, segmentation, restoration, etc.). They are particularly suited for image modeling, since *global* image characteristics can be conveniently specified by means of a few parameters that control *local* interactions. Most Gibbs random fields proposed in the literature however do not explicitly incorporate geometric information in image modeling. Since, success of an image processing algorithm depends on how well an image model represents known constraints (which are most frequently available in the form of geometric constraints), it would be beneficial to explicitly incorporate structural constraints in random image modeling.

A popular tool for image processing and analysis that considers geometric structure in images is *mathematical morphology* [9, 18]. In mathematical morphology, structuring elements (i.e., small templates with given shape and size) interact with images in order to extract shape/size information. This in-

teraction produces geometric information typical to the shape and size of the underlying structuring elements. Since mathematical morphology is a powerful image analysis tool for extracting and summarizing shape/size information, it is natural to express structural image constraints in terms of morphological operators. This leads to the idea of designing random field models that take into consideration geometric information using morphological constraints.

To accomplish this goal, a class of Gibbs random field models has been proposed in the literature [1, 2, 20, 22, 23] whose most probable realizations satisfy useful morphological constraints. In this paper, we provide a tutorial exposition that reveals the multiresolution nature of these models. We first provide reasons for why Gibbs random fields are good models for images. We then review morphological operators used to provide a multiresolution image decomposition. These operators allow efficient image representation by means of detail error signals. By appropriately constraining these signals, we obtain a Gibbs energy function with ground states that satisfy relevant geometric properties. We finally illustrate the potential of the proposed models with few examples.

2. Why Gibbs random fields?

As we mentioned in the introduction, Gibbs random fields are important statistical models for images. We now give a few reasons why this is so.

(a) Gibbs random fields are natural choices in image modeling.

Let us consider a two-dimensional discrete observation window $W = \{w \in \mathbb{Z}^2 \mid w = (m,n), 0 \le m \le M-1, 0 \le n \le N-1\}$, $1 \le M, N < \infty$, of $M \times N$ sites in $\mathbb{Z}^2$. Let $\mathbf{X}(w)$ be a random variable assigned at site $w \in W$ which takes values in a (discrete) state-space $\mathcal{R} = \{0, 1, \ldots, R\}$. The collection $\mathbf{X} = \{\mathbf{X}(w), w \in W\}$ is a two-dimensional *random field* on W which assumes realizations $X = \{X(w), w \in W\}$ in the Cartesian product $\mathcal{S} = \mathcal{R}^{MN}$. $\mathbf{X}$ can serve as a statistical model for discrete random images specified over a finite observation window W (which is the case in practice). If the probability mass function $\pi_T(X)$ of $\mathbf{X}$ is strictly positive, i.e., if

$$\pi_T(X) > 0, \quad \forall X \in \mathcal{S}, \tag{1}$$

then it is not difficult to show that

$$\pi_T(X) = \frac{1}{Z_T} \exp\{-\frac{1}{T} U(X)\}, \ \ \forall X \in \mathcal{S}, \tag{2}$$

where

$$Z_T = \sum_{X \in \mathcal{S}} \exp\{-\frac{1}{T} U(X)\} \tag{3}$$

(set $U(X) = -T \ln(\pi_T(X)/\pi_T(X_o))$, where X_o is the zero realization). In (2) and (3), U is a real-valued functional on $\mathcal{S}$, known as the *energy function*, such

that $U(X_o) = 0$, T is a real-valued positive constant, known as the *temperature*, whereas Z_T is a normalizing constant, which depends on the temperature T, known as the *partition function*. A probability mass function of the exponential form (2) is known as a *Gibbs distribution*. Any random field $\mathbf{X}$ whose probability mass function is of the form (2), (3) is known as a *Gibbs random field* (GRF).

It is now clear that, if we are interested in a stochastic image model with strictly positive probability distribution, then a Gibbs random field is the natural choice. The requirement that the *positivity condition* (1) is satisfied is usually not restrictive. This is a natural condition satisfied by all practical imaging systems. It simply states that any image in the state-space $\mathcal{S}$ may be a candidate realization for $\mathbf{X}$. However, this requirement may not be so natural when constraints are to be incorporated as forbidden states [16].

(b) Gibbs random fields allow modeling a wide spectrum of probability distributions.

It can be shown that, in the limit as $T \to \infty$, a GRF $\mathbf{X}$ becomes i.i.d.; i.e.,

$$\lim_{T \to \infty} \pi_T(X) = \frac{1}{|\mathcal{S}|}, \quad \forall X \in \mathcal{S} \ , \tag{4}$$

where $|A|$ denotes the *area* or *cardinality* of A. On the other hand, if

$$\mathcal{U} = \{X^g \in \mathcal{S} \mid U(X^g) \leq U(X), \quad \forall X \in \mathcal{S}\} \ , \tag{5}$$

then

$$\lim_{T \to 0^+} \pi_T(X) = \begin{cases} 1/|\mathcal{U}|, & \text{for } X \in \mathcal{U} \\ 0, & \text{otherwise} \end{cases} \ . \tag{6}$$

Therefore, the probability mass function of a GRF becomes uniform, over all global minima of its energy function (known as the *ground states* of $\mathbf{X}$), in the limit as the temperature decreases to zero. This demonstrates the fact that, although a GRF is specified by means of a simple exponential probability mass function of the form (2), (3), this function is capable of modeling a wide spectrum of random fields, ranging from purely random to purely deterministic, depending on the particular value of the temperature T.

We should point out here that it is the ground states of a Gibbs random field that are most important in image processing and analysis applications. This can be best explained by noticing that, at high temperatures, only short range pixel interactions are possible, as is clear from (4), where a typical GRF realization will be dominated by fine structure. However, at low enough temperatures and for large enough window W, long range pixel interactions are possible and a typical GRF realization will be dominated by large structures. This is nicely explained in [26]. Since at low enough temperatures the most probable states are the ground states, these will be the most interesting states from an image modeling point of view.

(c) Gibbs random fields can be easily used to incorporate constraints into image modeling.

Searching for a solution to an inverse problem may become easier by reducing the size of the search space. This may be accomplished by constraining candidate solutions to satisfy prespecified constraints. For example, given some a-priori knowledge about a candidate solution X, we may formalize this knowledge by requiring that X satisfies a constraint of the form $U(X) = 0$, for some well defined real-valued functional U on $\mathcal{S}$. In this case, instead of looking for a solution in space $\mathcal{S}$, we may look for a solution in the smaller space $\mathcal{S}' = \{X \in \mathcal{S} \mid U(X) = 0\}$. A Gibbs random field model, with energy function $U(X)$ can now be used to model $\mathbf{X}$. If $U(X) \geq 0$, for every $X \in \mathcal{S}$, it is not difficult to see that an image X satisfies the constraint $U(X) = 0$ if and only if it is a ground state. The problem of finding an X such that $U(X) = 0$ then reduces to the problem of finding one of the ground states of $\mathbf{X}$, a problem that can be solved by means of *simulated annealing* [5].

(d) Gibbs random fields may allow specification of global image characteristics by means of local interactions.

If, in addition to the positivity condition (4), the conditional probability of $\mathbf{X}(w)$, given the values of $\mathbf{X}$ at all sites in $W \setminus \{w\}$ ($A \setminus B = A \cap B^c$ is the set difference of B from A), depends only on the values of $\mathbf{X}$ at sites in $\mathcal{N}(w)$, i.e., if

$$\begin{aligned}\Pr[\mathbf{X}(w) = X(w) \mid \mathbf{X}(v) = X(v), v \in W \setminus \{w\}] \\ = \Pr[\mathbf{X}(w) = X(w) \mid \mathbf{X}(v) = X(v), v \in \mathcal{N}(w)],\end{aligned} \quad (7)$$

for every $w \in W$, where $\mathcal{N}(w)$ is a *neighborhood* of site w such that $w \notin \mathcal{N}(w)$ and $w \in \mathcal{N}(v) \Leftrightarrow v \in \mathcal{N}(w)$, then $\mathbf{X}$ is a *Markov random field* (MRF) on W with neighborhood $\mathcal{N}$. It can be shown that, in this case, $\mathbf{X}$ is a Gibbs random field whose energy function is specified by means of local interactions. It is however typical that, at low enough temperatures and large window W, a MRF experiences long range interactions. Therefore, a GRF that satisfies the Markovian condition (7) may allow specification of global image characteristics by means of local interactions.

Unfortunately, ground states obtained by means of traditional energy functions only satisfy simple geometrical constraints. In Section 4, a Gibbs random field is proposed whose ground states satisfy more complicated geometrical constraints, and in particular morphological constraints. These constraints are specified by means of a very useful multiresolution concept of mathematical morphology known as *granulometry* [3, 15].

3. Morphological Multiresolution Image Decomposition

In 1975, a seminal book by George Matheron, entitled *Random Sets and Integral Geometry*, appeared in the literature [15]. This book laid down the

foundations of a novel technique for shape processing and analysis known as *mathematical morphology*. It was subsequently popularized by the highly inspiring book *Image Analysis and Mathematical Morphology* by Jean Serra [18]. Today, mathematical morphology is considered to be a powerful tool for shape analysis. The main idea is to analyze shape by "probing" images with a small geometric template (e.g., line segment, disc, square) known as the *structuring element*. Choosing the appropriate structuring element strongly depends on the particular application at hand. This however should not be viewed as a limitation, since it usually leads to additional flexibility in algorithm design.

Although the original work on mathematical morphology was limited to binary images (shapes), it has been recently recognized (e.g., see [9]) that mathematical morphology can be extended to grayscale and other kinds of images. This can be done by considering mathematical morphology as a general algebraic tool that deals with operators on *complete lattices* (i.e., nonempty sets furnished with a partial order relationship $\leq$ for which every subset has an *infimum* and a *supremum*). In the following, we limit our interest to the complete lattice $\mathcal{X} = \mathrm{Fun}(\mathbb{Z}^2, \mathcal{R})$ of functions mapping $\mathbb{Z}^2$ into $\mathcal{R}$, furnished with the component-wise partial order relationship $X_1 \leq X_2 \Leftrightarrow X_1(w) \leq X_2(w)$, for every $w \in \mathbb{Z}^2$, $X_1, X_2 \in \mathcal{X}$, where $X_1 = \{X_1(w), w \in \mathbb{Z}^2\}$ and $X_2 = \{X_2(w), w \in \mathbb{Z}^2\}$. In this case, the supremum and infimum are defined by $[\bigvee_{i \in I} X_i](w) = \bigvee_{i \in I} X_i(w)$ and $[\bigwedge_{i \in I} X_i](w) = \bigwedge_{i \in I} X_i(w)$, for every $w \in \mathbb{Z}^2$, respectively. This however should not lead to the false conclusion that our discussion is limited to this case, since it can be easily extended to other situations as well. It is clear that $\mathcal{S} = \mathrm{Fun}(W, \mathcal{R}) \subset \mathcal{X}$.

An operator $\epsilon\colon\ \mathcal{X} \to \mathcal{X}$ is called an *erosion* if it satisfies $\epsilon(\bigwedge_{i \in I} X_i) = \bigwedge_{i \in I} \epsilon(X_i)$, for every collection $\{X_i \in \mathcal{X}, i \in I\}$ of elements in $\mathcal{X}$ (i.e., an operator on $\mathcal{X}$ that distributes over infima). On the other hand, an operator $\delta\colon\ \mathcal{X} \to \mathcal{X}$ is called a *dilation* if it satisfies $\delta(\bigvee_{i \in I} X_i) = \bigvee_{i \in I} \delta(X_i)$, for every collection $\{X_i \in \mathcal{X}, i \in I\}$ of elements in $\mathcal{X}$ (i.e., an operator on $\mathcal{X}$ that distributes over suprema). Two operators ϵ and δ are said to be an *adjunction* if $\delta(X_1) \leq X_2 \Leftrightarrow X_1 \leq \epsilon(X_2)$, for every $X_1, X_2 \in \mathcal{X}$. In this case, ϵ is an erosion and δ is a dilation. An operator γ is called an *opening* if it is *increasing* (i.e., $X_1 \leq X_2 \Rightarrow \gamma(X_1) \leq \gamma(X_2)$), *anti-extensive* (i.e., $\gamma(X) \leq X$), and *idempotent* (i.e., $\gamma(\gamma(X)) = \gamma(X)$). Dually, any operator ϕ that is increasing, idempotent, and *extensive* (i.e., $X \leq \phi(X)$) is called a *closing*. It is easy to show that, for an adjunction (ϵ, δ), the composition $\delta\epsilon$ (i.e., an erosion followed by a dilation) is an opening, whereas the composition $\epsilon\delta$ (i.e., a dilation followed by an erosion) is a closing.

From complete lattice-theoretic generalizations, it follows that any translation invariant erosion ϵ and any translation invariant dilation δ on $\mathcal{X}$ are of the form [9]

$$\epsilon(X)(w) \;=\; (X \ominus B)(w) \;=\; \bigwedge_{v \in \mathbb{Z}^2} [X(w+v) - B(v)], \quad \forall\, w \in \mathbb{Z}^2$$
$$\delta(X)(w) \;=\; (X \oplus B)(w) \;=\; \bigvee_{v \in \mathbb{Z}^2} [X(w-v) + B(v)], \quad \forall\, w \in \mathbb{Z}^2,$$

for some $B \in \mathcal{X}$, known as a *structuring function*. Moreover, erosion and

dilation by a structuring function B are *duals* of each other, in the sense that $X \oplus B = (X^* \ominus \check{B})^*$, where $X^*(w) = R - X(w)$ and $\check{B}(w) = B(-w)$, for every $w \in \mathbb{Z}^2$, and form an adjunction; i.e., $X \oplus B \leq Y \Leftrightarrow X \leq Y \ominus B$. Finally, if $B((0,0)) = 0$, then dilation is extensive, whereas erosion is anti-extensive.

Operators

$$\gamma(X) = \delta\epsilon(X) = (X \ominus B) \oplus B = X \circ B$$
$$\phi(X) = \epsilon\delta(X) = (X \oplus B) \ominus B = X \bullet B \ ,$$

are the translation invariant opening and closing by a structuring function B, respectively. Opening and closing are duals of each other, in the sense that $X \circ B = (X^* \bullet \check{B})^*$. Furthermore, they are nonlinear *smoothing operators*, in the sense that they eliminate signal variation in X and X^*, respectively, of "size" smaller than the "size" of the structuring function (e.g., see [13]).

One usually takes B to be constant over a bounded subset of $\mathbb{Z}^2$ with value $-\infty$ elsewhere. In such cases, the previous operators are known as *flat erosion*, *flat dilation*, *flat opening*, and *flat closing*, respectively, and the structuring function B is known as a *flat structuring function* (or structuring element). In this paper, we only deal with flat operators and flat structuring functions which take value 0 over bounded subsets of $\mathbb{Z}^2$.

In [3], [15], Delfiner and Matheron introduced a set of morphological operators known as *granulometry*. This is a parameterized family $\{\gamma_s\}_{s=0,1,...}$ of mappings, from $\mathcal{X}$ into itself, that satisfy the following four properties:

1. γ_0 is the identity mapping on $\mathcal{X}$, i.e., $\gamma_0(X) = X$, for every $X \in \mathcal{X}$.
2. γ_s is increasing, i.e., $X_1 \leq X_2 \Rightarrow \gamma_s(X_1) \leq \gamma_s(X_2)$, $s = 1, 2, ..., X_1, X_2 \in \mathcal{X}$.
3. γ_s is anti-extensive, i.e., $\gamma_s(X) \leq X$, $s = 1, 2, ...$, for every $X \in \mathcal{X}$.
4. $\gamma_s \gamma_r = \gamma_r \gamma_s = \gamma_{\max(s,r)}$, $s, r = 1, 2, ...$

It can be shown that $\{\gamma_s\}_{s=0,1,...}$ is a granulometry if and only if γ_0 is the identity mapping on $\mathcal{X}$ and $\{\gamma_s\}_{s=1,2,...}$ is a family of openings such that $r \geq s \Rightarrow \gamma_r \leq \gamma_s$. Granulometries are important since they can be used to generalize the concept of size. This can be easily seen in the binary case, when $\mathcal{R} = \{0, 1\}$ (in which case $\leq$, $\wedge$, $\vee$, X^* should be replaced by $\subseteq$, $\cap$, $\cup$, X^c, respectively). Notice that, as a direct consequence of Properties 1, 3 and 4 above, given a binary image X, $\{\gamma_0, \gamma_1, ...\}$ is a decreasing sequence, in the sense that

$$X = \gamma_0(X) \supseteq \gamma_1(X) \supseteq \gamma_2(X) \supseteq \cdots \supseteq \gamma_s(X) \supseteq \cdots \ .$$

When X consists of particles, $\gamma_s(X)$ can be viewed as a *sieve* of mesh width s that allows only particles of "size" less than s to pass through. In this case, we may say that a particle P of X is of "size" s if $P \cap \gamma_s(X) \neq \emptyset$ but

$P \cap \gamma_{s+1}(X) = \emptyset$. This leads to the observation that $\{\gamma_s(X), s = 0, 1, ...\}$ is a *multiresolution image decomposition scheme* which reduces "resolution" as s increases. However, the term "resolution" is not associated here to the frequency content of X, as is customary in linear multiresolution techniques (e.g., see [25]), but to its "size" content (see also [13]). Of course, the notion of "size" is vague at this point and strongly depends on the particular form of γ_s. In the following, however, we consider examples where the notion of "size" becomes specific.

Given a granulometry $\{\gamma_s\}_{s=0,1,...}$ on $\mathcal{X}$, the dual parameterized family $\{\phi_s\}_{s=0,1,...}$ of mappings on $\mathcal{X}$, with $\phi_s(X) = (\gamma_s(X^*))^*$, $s = 0, 1, ...$, is known as the *anti-granulometry* associated with $\{\gamma_s\}_{s=0,1,...}$. This definition allows extension of the concept of "size" to "negative sizes" in order to assure that both image foreground X and image background X^* are treated equally. Notice that $\{\phi_s\}_{s=0,1,...}$ is an anti-granulometry on $\mathcal{X}$ if and only if ϕ_0 is the identity operator and $\{\phi_s\}_{s=1,2,...}$ is a family of closings such that $r \geq s \Rightarrow \phi_r \geq \phi_s$. The concept of multiresolution image decomposition by means of granulometries can be extended to include anti-granulometries as well. We say that $\mathcal{M}(X)$ is a *granulometric multiresolution image decomposition* scheme, if

$$\mathcal{M}(X) = \{\ldots, \phi_2(X), \phi_1(X), X, \gamma_1(X), \gamma_2(X), ...\} .$$

EXAMPLE 3.1. The most widely used granulometry is obtained by setting $\gamma_s(X) = X \circ sB$, where B is a flat structuring function, and $sB = (s-1)B \oplus B$ with $0B((0,0)) = 0$ and $0B(w) = -\infty$, for $w \neq (0,0)$. If X is a binary image, it can be shown that $X \circ B = \bigcup_w \{B_w \mid B_w \subseteq X\}$, where $B_w = \{b + w \mid b \in B\}$ is the translation of structuring element B at point w (with slight abuse of notation, B denotes the support of the flat structuring function $B(w)$ as well; i.e., $B = \{w \in \mathbb{Z}^2 \mid B(w) = 0\}$ – we call B the *structuring element*). This shows that the opening of an image X by a structuring element B consists of the union of all translated replicas of B that fit inside X. Therefore, the opening $X \circ B$ is a *geometric filter* that eliminates all components of X that cannot include a translated replica of structuring element B. In this case, the notion of "size" is directly related to the structuring element B:

> *A particle P of X is of "size" s if there exists at least one translated replica of sB that fits inside P whereas there is no translated replica of $(s+1)B$ that fits inside P.*

This is illustrated in Figure 1 which depicts a binary image X and the components $\gamma_s(X) = X \circ sB$, $s = 1, 2, 3, 4$, of $\mathcal{M}(X)$, with B being a 7×7 square structuring element. The associated anti-granulometry is given by $\phi_s(X) = X \bullet s\check{B}$. □

EXAMPLE 3.2. An alternative granulometric multiresolution image decomposition scheme may be obtained by employing reduction in scale, in conformity to the standard multiresolution decomposition schemes associated with the theory

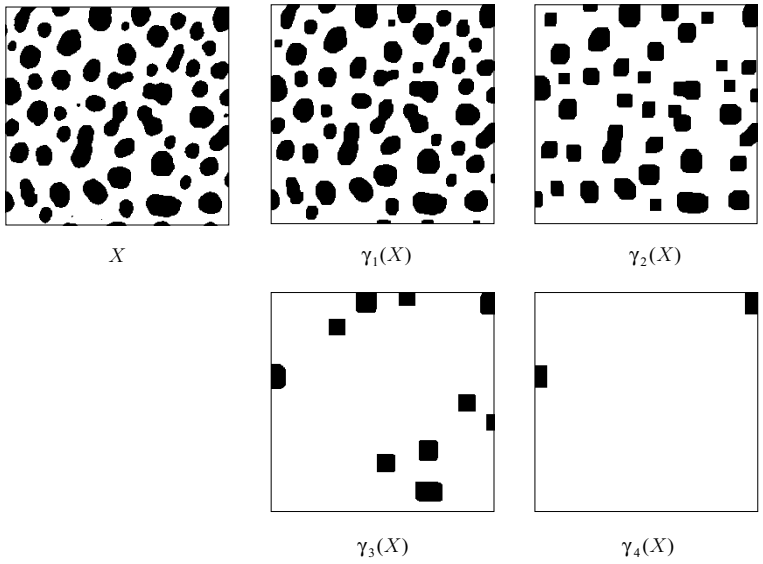

FIGURE 1. The components $\gamma_s(X) = X \circ sB$, $s = 0, 1, ..., 4$, of a granulometric multiresolution image decomposition scheme $\mathcal{M}(X)$ based on translation invariant openings. The structuring element B is taken to be a 7×7 square.

of wavelets and filter banks [25]. This produces a computationally advantageous image decomposition scheme. Roughly speaking, the time required for computing the decomposition $\mathcal{M}(X)$ of an $N \times N$ image by means of openings $X \circ sB$ and closings $X \bullet s\check{B}$ (assuming that B is a 3×3 structuring element) is of order N^4, whereas the time required for computing the decomposition proposed in this example is of order N^2. Let

$$\epsilon(X)(m,n) = \bigwedge_{(k,l)\in B} \{X(2m+k, 2n+l)\},\ \forall\,(m,n) \in \mathbb{Z}^2 \tag{8}$$

$$\delta(X)(m,n) = \bigvee_{(k,l)\in B} \{X(\frac{m-k}{2}, \frac{n-l}{2})\},\ \forall\,(m,n) \in \mathbb{Z}^2\ , \tag{9}$$

where B is a 3×3 square structuring element. In (9), $\frac{m-k}{2}$, $\frac{n-l}{2}$ are defined only for those values of m, n, k, l for which $(\frac{m-k}{2}, \frac{n-l}{2}) \in \mathbb{Z}^2$. It is not difficult to show that ϵ is an erosion, δ is a dilation, and (ϵ, δ) form an adjunction (in which case $\delta\epsilon$ is an opening and $\epsilon\delta$ is a closing). Notice that the erosion $\epsilon(X)$ increases the scale of signal X by a factor of 2, whereas the dilation $\delta(X)$ decreases scale by a factor of 2.

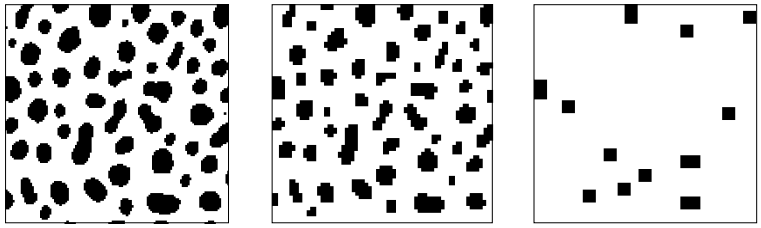

FIGURE 2. The components $\gamma_s(X), s = 1, 2, 3$, of a granulometric multiresolution decomposition scheme $\mathcal{M}(X)$ of the binary image of Fig. 1, based on the multiscale erosion and dilation in (8), (9). The structuring element B is taken to be a 3×3 square.

Set $\gamma_0(X) = \phi_0(X) = X$ and

$$\gamma_s(X) = \underbrace{\delta\delta\cdots\delta}_{s \text{ times}} \overbrace{\epsilon\epsilon\cdots\epsilon}^{s \text{ times}}(X), \text{ for } s = 1, 2, ...$$

$$\phi_s(X) = \underbrace{\epsilon\epsilon\cdots\epsilon}_{s \text{ times}} \overbrace{\delta\delta\cdots\delta}^{s \text{ times}}(X), \text{ for } s = 1, 2, ...$$

It can be shown that $\{\gamma_s\}_{s=0,1,...}$ is a family of openings such that $r \geq s \Rightarrow \gamma_r \leq \gamma_s$; therefore, it is a granulometry. The associated anti-granulometry is $\{\phi_s\}_{s=0,1,...}$. Notice that both $\gamma_s(X)$ and $\phi_s(X)$ preserve the scale of signal X. The opening γ_s is now a *multiscale filter* that eliminates all components of X that cannot include a replica of structuring element $(2^s - 1)B$ translated at a point $(2^s m, 2^s n)$ of $\mathbb{Z}^2$. In this case, the notion of "size" is directly related to scale:

> *A particle P of X is of "size" s if there exists at least one replica of $(2^s - 1)B$ translated at a point $(2^s m, 2^s n)$ of $\mathbb{Z}^2$ that fits inside P whereas there is no translated replica of $(2^{s+1} - 1)B$ that fits inside P.*

This is illustrated in Figure 2 which depicts the components $\gamma_s(X)$, $s = 1, 2, 3$, of $\mathcal{M}(X)$, with X being the binary image of Figure 1. □

EXAMPLE 3.3. Another granulometry can be constructed by gradually filtering out components of a binary image X with increasing area (see also [9]). Let $\text{conn}(X)$ denote the connected components of X (based on an assumed type of connectivity – for example, 4- connectivity). Define

$$\gamma_s(X) = \bigcup \{C \in \text{conn}(X) \mid |C| > \alpha(s)\} , \quad s \geq 0 , \tag{10}$$

where $\alpha(s)$ is a nonnegative increasing function of s, such that $\alpha(0) = 0$. It is not difficult to show that $\{\gamma_s\}_{s=0,1,...}$ is a family of openings such that

$r \geq s \Rightarrow \gamma_r \leq \gamma_s$; therefore, $\{\gamma_s\}_{s=0,1,...}$ is a granulometry. Operator γ_s is known as an *area opening*. In this case, the notion of "size" is directly related to the area:

A particle P of X is of "size" s if $\alpha(s) < |C| \leq \alpha(s+1)$.

This is illustrated in Figure 3 which depicts the components $\gamma_s(X)$, $s = 1, 2, ..., 5$, of $\mathcal{M}(X)$, with X being the binary image of Figure 1. We have assumed 4-connectivity and set $\alpha(s) = 30s^2$ in (10). □

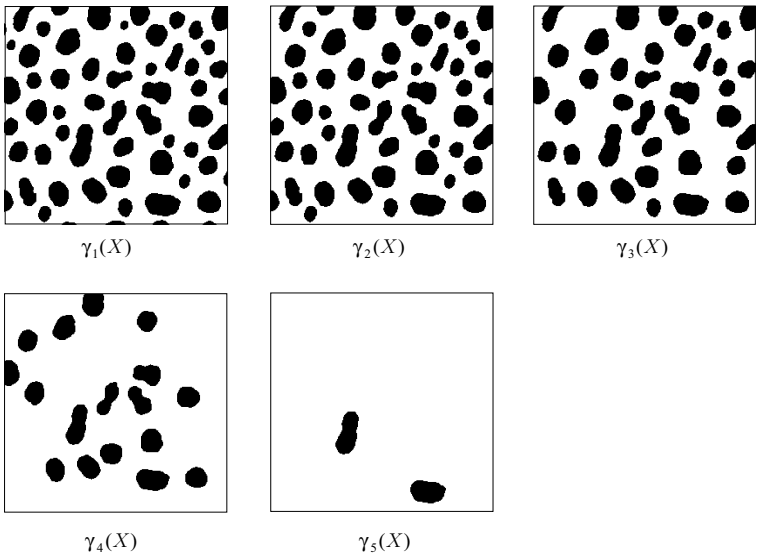

FIGURE 3. The components $\gamma_s(X)$, $s = 1, 2, ..., 5$, of a granulometric multiresolution decomposition scheme $\mathcal{M}(X)$ of the binary image of Fig. 1, based on area openings. A 4-connectivity is assumed and $\alpha(s) = 30s^2$ in (10).

Most often, instead of representing an image X by means of its multiresolution decomposition $\mathcal{M}(X)$, it is desirable to represent it by means of a decomposition

$$\mathcal{E}(X) = \{\ldots, \phi_2(X) - \phi_1(X), \phi_1(X) - X, X - \gamma_1(X), \gamma_1(X) - \gamma_2(X), ...\}$$

in terms of the *detail error images* $\phi_{s+1}(X) - \phi_s(X)$, $\gamma_s(X) - \gamma_{s+1}(X)$, for $s = 0, 1, ...$ The detail error image $\gamma_s(X) - \gamma_{s+1}(X)$ contains only particles that are of "size" s. Given $\{X - \gamma_1(X), \gamma_1(X) - \gamma_2(X), ...\}$, image X can be *exactly* reconstructed by a simple summation of the components $\gamma_s(X) - \gamma_{s+1}(X)$, $s = 0, 1, ...$ Therefore, $\{X - \gamma_1(X), \gamma_1(X) - \gamma_2(X), ...\}$ is an *invertible* decomposition of X. Furthermore, and in the binary case, $(\gamma_s(X) \setminus \gamma_{s+1}(X)) \cap (\gamma_{s+1}(X) \setminus \gamma_{s+2}(X)) = \emptyset$, for every $s = 0, 1, ...$; therefore, $\{X \setminus \gamma_1(X), \gamma_1(X) \setminus \gamma_2(X), ...\}$ is an *orthogonal* decomposition of X, in

addition to being invertible. By duality, similar remarks hold for the decomposition $\{\ldots, \phi_2(X) - \phi_1(X), \phi_1(X) - X\}$. Figures 4– 6 depict the decomposition $\{X \setminus \gamma_1(X), \gamma_1(X) \setminus \gamma_2(X), ...\}$ associated with the granulometries in Examples 3.1–3.3. Notice that union of all images in a given figure produces X.

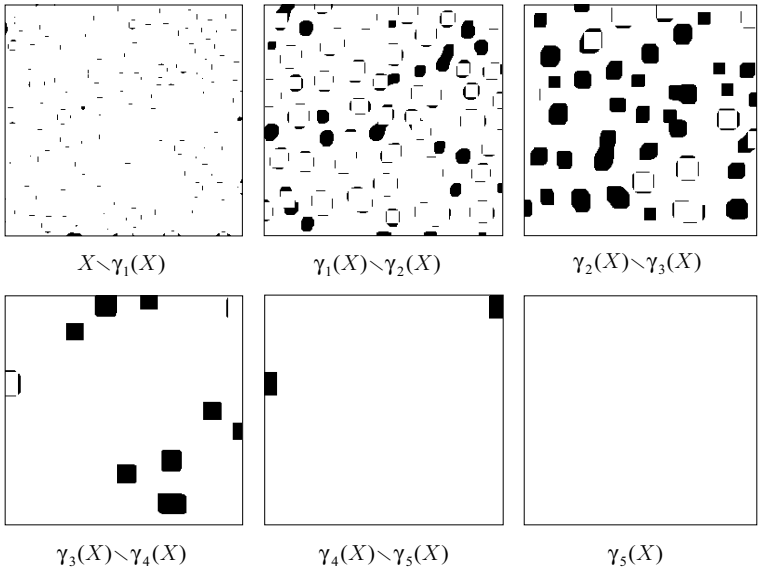

FIGURE 4. The decomposition $\{X \setminus \gamma_1(X), \gamma_1(X) \setminus \gamma_2(X), ...\}$ of image X in Fig. 1 associated with the granulometry in Example 3.1 (see also Fig. 1). The union of all these images produces X.

$\mathcal{E}(X)$ is frequently referred to as the (discrete) *size transform* of X. It can be thought of as a nonlinear analogue of the Fourier transform. One difference is that $\mathcal{E}(X)$ decomposes an image X in terms of its "size" content, whereas the Fourier transform decomposes X in terms of its frequency content. The *magnitude* $|\mathcal{E}(X)|$ of $\mathcal{E}(X)$ is given by

$$|\mathcal{E}(X)|(s) = \begin{cases} |\gamma_s(X) - \gamma_{s+1}(X)|, & \text{for } s = 0, 1, ... \\ |\phi_{|s|}(X) - \phi_{|s|-1}(X)|, & \text{for } s = -1, -2, ... \end{cases} \tag{11}$$

which is known as the *pattern spectrum* (in the grayscale case, when $R > 1$, $|X| = \sum_{w \in W} X(w)$). The pattern spectrum does not contain enough information to uniquely reconstruct X (in the same way that the magnitude Fourier transform is not adequate for signal reconstruction – this also requires knowledge of phase information). It is however a powerful tool for shape description. For example, if $\gamma_s(X) = X \circ sB$ (as in Example 3.1) and if $|\mathcal{E}(X)|(0) = 0$, then $X = X \circ B$. In the binary case, this means that X is a union of translated replicas of structuring element B. On the other hand, if $\gamma_s(X)$ is as in Example 3.3, $|\mathcal{E}(X)|(s) = 0$, for $s = 0, 1$, results in $X = \gamma_1(X) = \gamma_2(X)$, which means that X contains no components with area less than $\alpha(2)$.

In the next section, we show that the pattern spectrum can be effectively

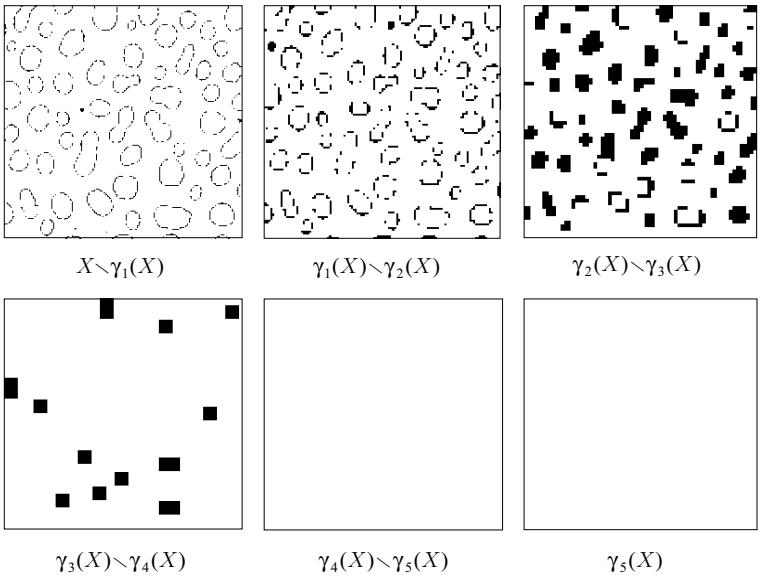

FIGURE 5. The decomposition $\{X \smallsetminus \gamma_1(X), \gamma_1(X) \smallsetminus \gamma_2(X), ...\}$ of image X in Fig. 1 associated with the granulometry in Example 3.2 (see also Fig. 2). The union of all these images produces X.

used for random image modeling. The key is to consider a parametric Gibbs random field with energy function specified by means of the pattern spectrum and recognize that the pattern spectrum of the ground states of such a model is directly related to the model parameters.

4. STATISTICAL MODELS

As we discussed in the introduction, our main task is to construct random image models which incorporate a priori geometric information in the form of morphological constraints. If we make the "benign" assumption that the probability mass function is strictly positive, then our model should necessarily be a GRF. As a direct consequence of (4), a GRF at high temperatures experiences only short range pixel interactions and a typical realization lacks structure. However, at low enough temperatures and for a large enough window W, long range pixel interactions are possible and a typical GRF realization is well structured. Since, at low enough temperatures, the most probable states of a GRF are its ground states (recall (5), (6)), these are the most interesting states from a practical point of view. We are therefore interested in random images modeled as GRFs whose ground states satisfy certain morphological constraints. In the following, we present a family of GRFs whose ground states are specified

by means of the pattern spectrum.

Consider a GRF whose energy function is given by [20, 23]

$$\begin{aligned} U(X) &= \sum_{i=0}^{I} a_i \Big| |\gamma_i(X) - \gamma_{i+1}(X)| - \nu_i \Big| \\ &+ \sum_{j=1}^{J} a_{-j} \Big| |\phi_j(X) - \phi_{j-1}(X)| - \nu_{-j} \Big|, \quad \forall X \in \mathcal{S}. \end{aligned} \tag{12}$$

In (12), $\{\gamma_s\}_{s=0,1,...}$ is a granulometry, $\{\phi_s\}_{s=0,1,...}$ is its associated anti-granulometry, $I \geq 0$, $J \geq 1$ are two finite integers, $\{a_i, -J \leq i \leq I\}$ are binary-valued parameters, taking values 0 or 1, and $\{\nu_i, -J \leq i \leq I\}$ are real-valued nonnegative parameters such that

$$\sum_{i=-J}^{I} \nu_i \leq R|W|. \tag{13}$$

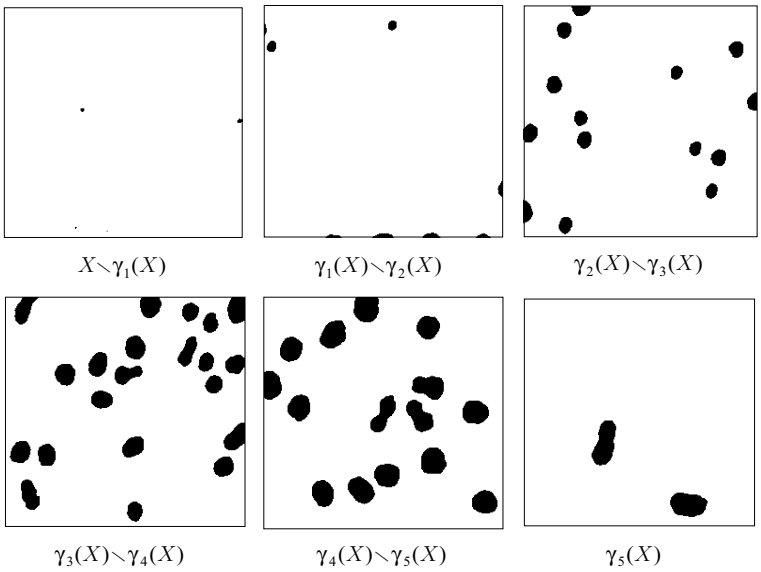

FIGURE 6. The decomposition $\{X \setminus \gamma_1(X), \gamma_1(X) \setminus \gamma_2(X), ...\}$ of image X in Fig. 1 associated with the granulometry in Example 3.3 (see also Fig. 3). The union of all these images produces X.

From (5), (11), and (12), it is not difficult to see that (we assume here that the granulometry γ and the parameters I, J, a, ν in (12) are chosen so that $\mathcal{U} \neq \emptyset$)

$$\mathcal{U} = \{X^g \in \mathcal{S} \mid |\mathcal{E}(X^g)|(s) = \nu_s, \ \forall\, s : a_s = 1\}.$$

Therefore, the pattern spectrum of the ground states of the GRF with energy function (12) is constrained to take the value ν_s at sizes s for which $a_s = 1$. In this case, and at low enough temperatures, the resulting GRF $\mathbf{X}$ may favor realizations whose pattern spectrum is determined by the particular values of a's and ν's. Notice that $\sum_{s=-\infty}^{\infty} |\mathcal{E}(X)(s)| = R|W|$, which implies that the parameters ν in (12) should satisfy condition (13).

The resulting GRF is not in general locally Markov (i.e., (7) is not satisfied for a small neighborhood $\mathcal{N}$) [20, 23]. This deviates from the common belief that only GRFs that satisfy a local Markovian condition should be considered for image modeling (however, see [7] for an exception). We however believe that the main reason for using locally specified GRFs, as opposed to using more general GRFs, is purely computational. A local Markovian assumption simplifies simulation by means of *Markov chain Monte Carlo* (MCMC) sampling [6]. MCMC sampling is an iterative simulation technique that relies heavily on computing energy differences $\Delta U_k = U(X^{(k)}) - U(X^{(k-1)})$ at each iteration, where $X^{(k)}$ is the image obtained at iteration k. When $\mathbf{X}$ is a MRF, ΔU_k has a simple "local" form which can be easily computed. However, depending on the particular choice for the granulometry $\{\gamma_s\}_{s=0,1,\ldots}$ in (12), ΔU_k may also be put in a "local" form, and fast MCMC sampling algorithms may be designed despite the fact that $\mathbf{X}$ is not locally Markov. We do not want to expand on these subjects here, since they can get quite technical. For more information, the interested reader is referred to [20, 23]. In the following, we prefer to illustrate the proposed model with two examples.

EXAMPLE 4.1. A GRF with energy function given by (12) can be effectively used to statistically model a certain type of geometric constraints. For example, we may be interested in random field models that favor realizations that are both open and closed with respect to a structuring element B. This means that the model of interest is capable of assigning higher probabilities to realizations for which both foreground and background are unions of translated replicas of B, whereas assigning lower probabilities to realizations that violate such a condition. As we see in the next example, a model of this type is useful for regularizing the inverse problem of removing noise from degraded images.

In (12), if we set $I = 0$, $J = 1$, $a_{-1} = a_0 = 1$, $\nu_{-1} = \nu_0 = 0$, and $\gamma_s(X) = X \circ sB$ (in which case $\phi_s(X) = X \bullet s\check{B}$), then

$$U(X) = |X \bullet \check{B} - X| + |X - X \circ B| \ , \forall \, X \in \mathcal{S} \ , \tag{14}$$

in which case, the ground states will be both open and closed with respect to B. As the temperature T decreases to zero, the GRF probability mass function with energy function (14) will cluster around the ground states of U. At low enough temperatures, the resulting GRF will strongly favor realizations that are both open and closed with respect to the structuring element B. Figure 7(a) depicts a realization X of a binary GRF with energy function (14), where B is a 13×13 pixel square structuring element, sampled at a low temperature ($T = 0.1$). The square structure of both foreground and background is a direct

consequence of the fact that X is approximately open and closed with respect to B. A similar realization is depicted in Figure 7(b). In this case however B is a discrete approximation of a disk.

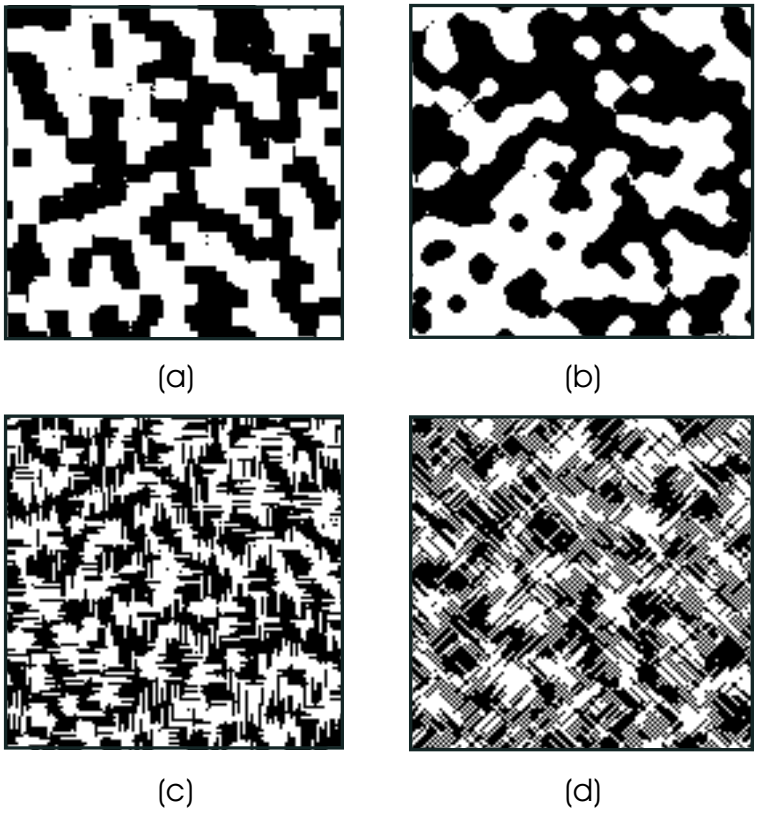

FIGURE 7. Realizations of binary GRFs whose energy function is given by (12) with appropriately chosen parameters. The depicted images are approximately both open and closed with respect to given structuring elements.

Other interesting realizations can be obtained by using the granulometries considered in Examples 3.2, 3.3. However, a number of interesting patterns can also be obtained by means of extending the granulometry of Example 3.1 to the case when

$$\gamma_s(X) = \bigvee_{k=1}^{K} X \circ sB^{(k)} \ , \quad \forall\, X \in \mathcal{S} \ , \tag{15}$$

in which case

$$\phi_s(X) = \bigwedge_{k=1}^{K} X \bullet s\check{B}^{(k)} \ , \quad \forall\, X \in \mathcal{S} \ , \tag{16}$$

for some integer $K \geq 1$. In (15), (16), $\{B^{(k)}, k = 1, 2, ..., K\}$ is a collection of

structuring elements. Figures 7(c) and 7(d) depict two realizations of a binary GRF with energy function

$$U(X) = |(X \bullet \check{B}^{(1)}) \wedge (X \bullet \check{B}^{(2)}) - X| + |X - (X \circ B^{(1)}) \vee (X \circ B^{(2)})|,$$

for all $X \in \mathcal{S}$, at temperature $T = 0.1$. For Figure 7(c), $B^{(1)}$ is a vertical linear structuring element of length 6, whereas $B^{(2)}$ is a horizontal linear structuring element of the same length. For Figure 7(d), the structuring elements are the ones in Figure 7(c) rotated by 45^o. More details on these and other examples can be found in [20, 23]. □

EXAMPLE 4.2. In many image processing and analysis applications, image data X are corrupted by noise and clutter. In this case, we are interested in designing an operator Ψ which, when applied on the corrupted data Y, *optimally* recovers X. For illustration purposes, let us limit ourselves to the binary case. We may assume that X is corrupted by *union-intersection noise*, in which case

$$Y = (X \cap N_1^c) \cup N_2 \ , \tag{17}$$

where N_1, N_2 are the *intersection* and *union* noise components, respectively. The inverse problem of recovering X from Y can be solved by means of an operator Ψ, such that

$$\hat{X} = \Psi(Y) = \Psi((X \cap N_1^c) \cup N_2) \tag{18}$$

is a "good" approximation to X. The effectiveness of obtaining X from Y by means of Ψ strongly depends on certain "non-overlapping" characteristics of the noise free image X and the noise components N_1, N_2, typical to the particular filtering problem at hand. It also depends on the effectiveness of Ψ in discriminating between these characteristics. For example, if we assume that the noise-free image X is "lowpass," whereas the noise components N_1 and N_2 are sufficiently "highpass" (in the sense that the "frequency bands" of X and N_1, N_2 do not overlap), then an "ideal low pass" filter with appropriate "cut-off frequency" will perfectly reconstruct X from Y. To obtain such a filter, we certainly need to define what we mean by "lowpass," "highpass," "frequency bands," etc., and make the *regularizing assumption* that (17) is limited to "lowpass" images X. Notice however that Ψ should be such that $\Psi(X) = X$, which guarantees that Ψ does not affect X when $N_1 = N_2 = 0$. Clearly, this condition should not hold for every X (otherwise, Ψ will be the identity operator). It should however hold for all "lowpass" images. In general, the *invariance domain* of Ψ (i.e., the collection of all images X for which $\Psi(X) = X$), may contain images that are not necessarily "lowpass." It is therefore desirable to consider only operators Ψ with the property that any "lowpass" image X belongs to its invariance domain.

To be more specific, we should note here that the union and intersection noise components are usually "bandlimited," in the sense that there exists a "size" s_0 such that

$$|\mathcal{E}(N_1)|(s) = |\mathcal{E}(N_2)|(s) = 0 \ , \quad \text{for } s \geq s_0 \ . \tag{19}$$

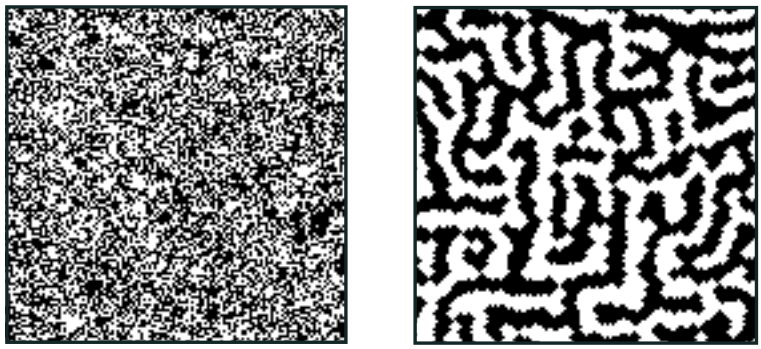

$T = 5.0$ $T = 0.1$

FIGURE 8. Realizations of a GRF with energy function (21), with $s_0 = 2$, $B = \{(0,-1), (0,0), (0,1), (-1,0), (1,0)\}$, at temperatures $T = 5.0, 0.1$.

This simply says that the "size" of the noise components is small, limited between 0 and $s_0 - 1$. If we consider "size" as being the discriminating factor between X and N_1, N_2, then the noise free image X should be "bandlimited" as well, in the sense that

$$|\mathcal{E}(X)|(s) = 0 \ , \quad \text{for } -s_0 \leq s \leq s_0 - 1 \ . \tag{20}$$

To guarantee (20), we may assume that X is a realization of a GRF $\mathbf{X}$ whose energy function is given by (12), with $I = s_0 - 1$, $J = s_0$, $a_{-s_0} = a_{-s_0+1} = \cdots = a_0 = a_1 = \cdots = a_{s_0-1} = 1$, $\nu_{-s_0} = \nu_{-s_0+1} = \cdots = \nu_0 = \nu_1 = \cdots = \nu_{s_0-1} = 0$, $\gamma_s(X) = X \circ sB$, and $\phi_s(X) = X \bullet s\check{B}$. In this case,

$$U(X) = |X \bullet s_0\check{B} \smallsetminus X| + |X \smallsetminus X \circ s_0 B| \ , \quad \forall X \in \mathcal{S} \ , \tag{21}$$

and the ground states consist of all binary images X on W which are both open and closed with respect to structuring element $s_0 B$ (i.e., $X = X \circ s_0 B = X \bullet s_0\check{B}$). This implies that, at low enough temperatures, the probability mass function of $\mathbf{X}$ will assign higher probabilities to images that are both open and closed with respect to structuring element $s_0 B$ and a typical realization will be an image X that approximately satisfies the desirable condition (20).

Figure 8 depicts two 128×128 pixel realizations of such a GRF with $T = 5.0$ and $T = 0.1$. We have set $s_0 = 2$ and $B = \{(0,-1), (0,0), (0,1), (-1,0), (1,0)\}$. At the high temperature $T = 5.0$, the realization looks random, whereas, at the low temperature $T = 0.1$, the realization is well structured and satisfies the following geometric property:

> *Both foreground and background are approximately unions of translated replicas of structuring element* $2B$.

This is a direct consequence of the fact that the realization is approximately open and closed with respect to structuring element $2B$.

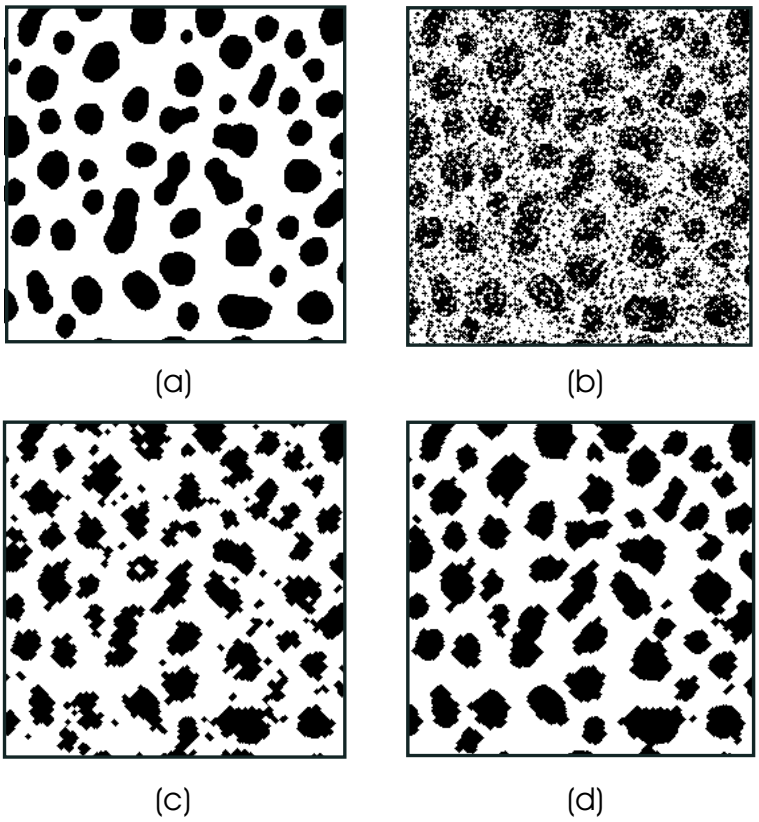

FIGURE 9. (a) A binary image X whose pattern spectrum is approximately zero at "sizes" $-2 \leq s \leq 1$. (b) A noisy version of the image in (a) – the SNR is 3.10 dB. (c) The result of applying the alternating sequential filter (22), with $s_0 = 2$, on the image in (b) – the SNR is 10.46 dB. (d) The result of applying the morphological filter (23), with $s_0 = 2$, on the image in (b) – the SNR is 14.98 dB.

It can be shown (e.g., see [21]) that, if X in (17) is a realization of a GRF $\mathbf{X}$ with energy function (21) at low enough temperature, and if the pattern spectra in (19), (20) are based on the granulometry of Example 3.1, then a desirable operator Ψ in (18) will be the *alternating sequential filter* [17, 19]

$$\Psi(Y) = (((((Y \circ B) \bullet \check{B}) \circ 2B) \bullet 2\check{B}) \circ \cdots \circ s_0 B) \bullet s_0 \check{B} \ . \tag{22}$$

Notice that, if (20) is satisfied, then $X = X \circ sB = X \bullet s\check{B}$, for every $1 \leq s \leq s_0$ and X will belong to the invariance domain of Ψ, as required. Figure 9(a) depicts a binary image X for which (20) is satisfied. The corresponding noisy image, depicted in Figure 9(b), is obtained by means of (17) with N_1, N_2 being realizations of a *germ-grain model* [24]. In this case, a number of points (the *germs*) in W are chosen at random. A structuring element nB (the *grain*),

with $B = \{(0,-1),(0,0),(0,1),(-1,0),(1,0)\}$, is centered at each germ, with n taking values 0 or 1 with equal probability. If no much overlapping occurs among the noise grains, then (19) will be approximately satisfied (with $s_0 = 2$) for both N_1 and N_2. For the noisy image depicted in Figure 9(b) the *signal to noise ratio* (SNR) $20\log_{10}(|X|/|Y \triangle X|)$ is 3.10 dB ($\triangle$ denotes *symmetric difference*, i.e., $X_1 \triangle X_2 = (X_1 \setminus X_2) \cup (X_2 \setminus X_1)$). Application of the alternating sequential filter (22), with $B = \{(0,-1),(0,0),(0,1),(-1,0),(1,0)\}$ and $s_0 = 2$, produces the approximation $\hat{X}$ depicted in Figure 9(c). $\hat{X}$ is a reasonable approximation of X, despite the fact that the input SNR is rather low. In fact, the SNR in Figure 9(c) is 10.46 dB, an increase of 7.36 dB from the SNR of Figure 9(b).

An alternative operator Ψ can be obtained by setting

$$\Psi(Y) = (\rho_{B_0}(Y \bigcirc s_0 B \mid Y) \bullet s_0 \check{B}) \bigcirc s_0 B \ , \tag{23}$$

where

$$\rho_{B_0}(X_m \mid X) = \bigcup_{n \geq 1} \delta^n_{B_0}(X_m \mid X) \ , \tag{24}$$

$$\delta^n_{B_0}(X_m \mid X) = \delta^1_{B_0} \delta^1_{B_0} \cdots \delta^1_{B_0}(X_m \mid X) \quad (n \text{ times}) \ , \tag{25}$$

$$\delta^1_{B_0}(X_m \mid X) = (X_m \oplus B_0) \cap X, \ X_m \subseteq X \ . \tag{26}$$

Operator $\delta^n_{B_0}(X_m \mid X)$ in (25), (26) is known as the *conditional dilation* of X_m in X of size n. The conditional dilation "expands" a *marker* X_m of X by means of a structuring element B_0 (that contains the origin), making sure that the "expansion" remains always inside X. Operator $\rho_{B_0}(X_m \mid X)$ in (24) is known as *morphological image reconstruction*. Its effect is to recover all connected components of image X marked by a marker X_m [9]. The opening $Y \bigcirc s_0 B$ in (23) removes all components of Y of "size" less than s_0. It will therefore eliminate most of N_2 in (17). However, it will also distort $X \cap N_1^c$. The morphological reconstruction $\rho_{B_0}(Y \bigcirc s_0 B \mid Y)$ will reconstruct the connected components of Y marked by $Y \bigcirc s_0 B$, and it will therefore reconstruct most of $Y \cap N_1^c$ (notice that $Y \bigcirc s_0 B \subseteq Y$, as required for $Y \bigcirc s_0 B$ to be a marker of Y). However, $\rho_{B_0}(Y \bigcirc s_0 B \mid Y)$ may also reconstruct components of N_2 that "touch" X. Subsequent closing with structuring element $s_0 B$ will remove most of N_1 from $X \cap N_1^c$, whereas opening with $s_0 B$ will remove most components of N_2 that "touch" X. This is illustrated in Figure 10, and for the noisy image depicted in Figure 9(b), with $B = \{(0,-1),(0,0),(0,1),(-1,0),(1,0)\}$. The resulting operator is a variant of an *open-close-open* morphological filter [19], where the first opening is replaced by operator $\rho_{B_0}(Y \bigcirc s_0 B \mid Y)$. In fact, $\rho_{B_0}(Y \bigcirc s_0 B \mid Y)$ is an opening as well, known as *opening by reconstruction* [19]. If (20) is satisfied, then $X = X \bigcirc sB = X \bullet s\check{B}$, for every $1 \leq s \leq s_0$ and X will belong to the invariance domain of Ψ, as required. This is a direct consequence of the fact that $\rho_{B_0}(X \mid X) = X$.

Application of this operator on the noisy image depicted in Figure 9(b), with $B = B_0 = \{(0,-1),(0,0),(0,1),(-1,0),(1,0)\}$ and $s_0 = 2$, produces the

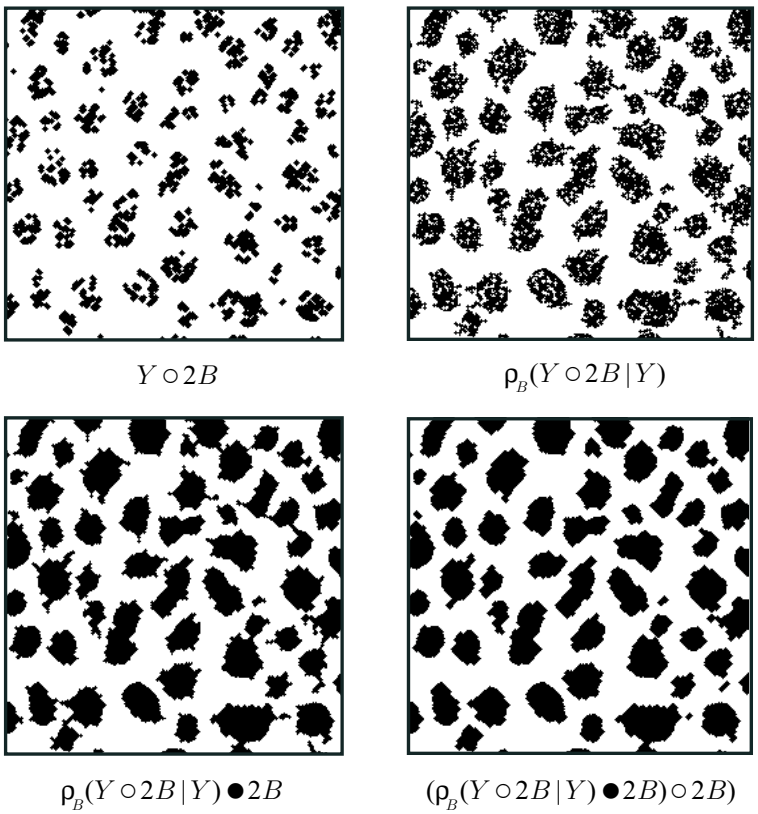

FIGURE 10. Illustration of the steps required for the implementation of operator (23).

approximation $\hat{X}$ depicted in Figure 9(d). $\hat{X}$ is a better approximation to X than the one obtained by means of alternating sequential filtering, as is evident by comparing (c) and (d) in Figure 9. In fact, the SNR in Figure 9(d) is 14.48 dB, an increase of 11.38 dB from the SNR of Figure 9(b) and 4.02 dB from the SNR of Figure 9(c). □

5. CONCLUSION

In this paper, we have considered the problem of statistical image modeling by directly incorporating multiresolution morphological constraints in the probability mass function of a random image model. This was achieved by considering a class of Gibbs random fields, with energy function given by (12), whose most likely realizations satisfy the desirable constraints.

An important issue here is development of efficient algorithms for simulating these models. It has been shown in [20, 23] that a Markov chain Monte Carlo sampling technique exists that allows fast simulation when the granulometry

associated with (12) is the one in Example 3.1. It will be very important to develop sampling algorithms for other granulometric choices, especially for the choice in Example 3.2, which provides multiresolution signal decomposition by reducing scale as well.

Important statistical properties of the proposed models have been extensively studied in [20, 23]. It has been also demonstrated, by means of texture classification experiments, that the proposed models are very useful in modeling natural textures. We believe that the proposed models can be effectively used as a-priori models in Bayesian image restoration as well. Their use in this framework is currently under investigation.

Finally, it is worthwhile noticing that additional models may be constructed, more appropriate for a particular application, by appropriately choosing the granulometry in (12). Extension of the proposed models to the continuous case is another exciting possibility. This has been recently explored in [11, 12].

References

1. Chen, F. (1994). *Robust and Morphologically Constrained Image Segmentation.* PhD Thesis, Department of Electrical and Computer Engineering, University of Massachusetts at Amherst, Amherst, Massachusetts.
2. Chen, F., Kelly, P. A. (1992). Algorithms for generating and segmenting morphologically smooth binary images. *Proceedings of the 26th Conference on Information Sciences and Systems,* 902–906.
3. Delfiner, P. (1971). A generalization of the concept of size. *Journal of Microscopy* **95**, 203–216.
4. Geman, D. (1990). Random fields and inverse problems in imaging. *École d'Été de Probabilités de Saint-Flour XVIII - 1988*, P. L. Hennequin, Ed., **1427**. Springer-Verlag, Berlin, Germany, 117–193.
5. Geman, S., Geman, D. (1984). Stochastic relaxation, Gibbs distributions, and the Bayesian restoration of images. *IEEE Transactions on Pattern Analysis and Machine Intelligence* **6**, 721–741.
6. Geyer, C. J. (1992). Practical Markov chain Monte Carlo (with discussion). *Statistical Science* **7**, 473–511.
7. Gimel'farb, G. L. (1996). Texture modeling by multiple pairwise pixel interactions. *IEEE Transactions on Pattern Analysis and Machine Intelligence* **18**, 1110–1114.
8. Hadamard, J. (1923). *Lectures on the Cauchy Problem in Linear Partial Differential Equations.* Yale University Press, New Haven, Connecticut.
9. Heijmans, H. J. A. M. (1994). *Morphological Image Operators.* Academic Press, Boston, Massachusetts.
10. Jain, A. K. (1989). *Fundamentals of Digital Image Processing.* Prentice Hall, Englewood Cliffs, New Jersey.
11. van Lieshout, M. N. M. (1997). *Size distributions in stochastic geometry.* Tech. Rep. PNA-R9715, CWI, Amsterdam, The Netherlands. To appear in *Pattern Recognition.*

12. VAN LIESHOUT, M. N. M. (1998). Size-based random closed sets. *Mathematical Morphology and Its Applications to Image Processing*, H. J. A. M. HEIJMANS and J. B. T. M. ROERDINK, Eds. Kluwer, Dordrecht, The Netherlands 291–298.
13. MARAGOS, P. (1989). Pattern spectrum and multiscale shape representation. *IEEE Transactions on Pattern Analysis and Machine Intelligence* **11**, 701–716.
14. MARROQUIN, J., MITTER, S., POGGIO, T. (1987). Probabilistic solution of ill-posed problems in computational vision. *Journal of the American Statistical Association* **82**, 76–89.
15. MATHERON, G. (1975). *Random Sets and Integral Geometry.* John Wiley, New York City, New York.
16. MOUSSOURIS, J. (1974). Gibbs and Markov random systems with constraints. *Journal of Statistical Physics* **10**, 11–33.
17. SCHONFELD, D., GOUTSIAS, J. (1991). Optimal morphological pattern restoration from noisy binary images. *IEEE Transactions on Pattern Analysis and Machine Intelligence* **13**, 14–29.
18. SERRA, J. (1982). *Image Analysis and Mathematical Morphology.* Academic Press, London, England.
19. SERRA, J., VINCENT, L. (1992). An overview of morphological filtering. *Circuits, Systems and Signal Processing* **11**, 47–108.
20. SIVAKUMAR, K. (1997). *Morphological Analysis of Random Fields: Theory and Applications.* PhD Thesis, Department of Electrical and Computer Engineering, The Johns Hopkins University, Baltimore, Maryland.
21. SIVAKUMAR, K., GOUTSIAS, J. (1997). Discrete morphological size distributions and densities: Estimation techniques and applications. *Journal of Electronic Imaging* **6**, 31–53.
22. SIVAKUMAR, K., GOUTSIAS, J. (1997). Morphologically constrained discrete random sets. *Advances in Theory and Applications of Random Sets*, D. JEULIN, Ed. World Scientific, Singapore 49–66.
23. SIVAKUMAR, K., GOUTSIAS, J. (1997). *Morphologically constrained Gibbs random fields: Applications to texture synthesis and analysis.* Tech. Rep. JHU/ECE 97-11, Department of Electrical and Computer Engineering, The Johns Hopkins University, Baltimore, MD.
24. STOYAN, D., KENDALL, W. S., MECKE, J. (1995). *Stochastic Geometry and its Applications, Second Edition.* John Wiley, Chichester, England.
25. VETTERLI, M., KOVACEVIC, J. (1995). *Wavelets and Subband Coding.* Prentice Hall, Englewood Cliffs, New Jersey.
26. WILSON, K. G. (1979). Problems in physics with many scales of length. *Scientific American* **24**, 158–177.